Journal of
Intelligent Material
Systems and Structures

Original Article

Journal of Intelligent Material Systems and Structures
1–13

DOI: 10.1177/1045389X19836172
journals.sagepub.com/home/jim
SAGE

Design, modeling, and evaluation of a slim haptic actuator based on electrorheological fluid

Alex Mazursky[1], Jeong-Hoi Koo[1] and Tae-Heon Yang[2]

Abstract

Realistic haptic feedback is needed to provide information to users of numerous technologies, such as virtual reality, mobile devices, and robotics. For a device to convey realistic haptic feedback, two touch sensations must be present: tactile feedback and kinesthetic feedback. Although many devices today convey tactile feedback through vibrations, most neglect to incorporate kinesthetic feedback. To address this issue, this study investigates a haptic device with the aim of conveying both kinesthetic and vibrotactile information to users. A prototype based on electrorheological fluids was designed and fabricated. By controlling the electrorheological fluid flow via applied electric fields, the device can generate a range of haptic sensations. The design centered on an elastic membrane that acts as the actuator's contact surface. Moreover, the control electronics and structural components were integrated into a compact printed circuit board, resulting in a slim device suitable for mobile applications. The device was tested using a dynamic mechanical analyzer to evaluate its performance. The device design was supported with mathematical modeling and was in agreement with experimental results. According to the just-noticeable difference analysis, this range is sufficient to transmit distinct kinesthetic and vibrotactile sensations to users, indicating that the electrorheological fluid–based actuator is capable of conveying haptic feedback.

Keywords

Haptic actuator, electrorheological fluid, fluid interface, kinesthetic, tactile

1. Introduction

In recent years, mobile devices have experienced a shift from mechanical buttons to smooth, touch screen keyboards. However, the benefit of larger and more versatile screens comes at a cost to the physical feedback associated with indenting buttons. The information conveyed to the user through these touch sensations is referred to as haptic feedback. In addition to visual and auditory sensations, being able to touch, feel, and manipulate objects in an environment, whether real or virtual, offers the user a greater sense of immersion (Srinivasan and Basdogan, 1997). Therefore, haptic feedback is desired for numerous applications including simulators, teleoperation, entertainment, and more (Coles et al., 2011; Laycock and Day, 2003; Park and Khatib, 2006). To emulate and restore physical feedback in electronics, haptic technologies are being investigated and applied to bridge the gap between the user and the virtual world. Comprehensive haptic feedback comprises two components: (1) kinesthetic feedback and (2) tactile feedback. Kinesthetic feedback provides information about position and movement of joints and muscles. Tactile feedback consists of the sensations felt at the surface of one's skin and just underneath it. When examining an object, humans may rub it to feel its texture and roughness (tactile sensation) and press it to feel its resistance and elasticity (kinesthetic sensation). Therefore, both sensations must be present to completely observe an object through touch (Srinivasan and Basdogan, 1997).

Although the implementation of miniature vibrotactile actuators has been extensive, the development of small-scale kinesthetic actuators has been relatively slow. Research toward kinesthetic devices generally uses alternating current/direct current (AC/DC) motors as the working principle to generate force feedback

[1]Department of Mechanical and Manufacturing Engineering, Miami University, Oxford, OH, USA
[2]Department of Electrical Engineering, Korea National University of Transportation, Chungju, Republic of Korea

Corresponding author:
Jeong-Hoi Koo, Department of Mechanical and Manufacturing Engineering, Miami University, 56M EGB, Oxford, OH 45056, USA.
Email: koo@miamioh.edu

sensations (Bianchi et al., 2009; Fujita and Ohmori, 2001; Song et al., 2005). However, AC/DC motor-based actuators cannot be easily integrated into mobile devices due to their size and power consumption. Furthermore, active-controlled motors have been found to have issues with instability, making certain haptic applications less feasible (Adams et al., 1998; An and Kwon, 2006).

To avoid the problems associated with motors, many researchers have investigated actuating haptic sensations through the adjustable properties of smart materials, which pose a mechanically simpler solution to traditional actuation. Piezoelectric beams are a popular means of producing vibrotactile feedback at mobile scale, such as in *Touch Engine* (Poupyrev et al., 2002; Poupyrev and Maruyama, 2003; Rekimoto and Schwesig, 2006). Shape memory alloy wires have been applied to variable stiffness deformable interfaces, such as in *MimicTile* and *Morphees* (Nakagawa et al., 2012; Roudaut et al., 2013). However, neither *Touch Engine* nor *MimicTile*/*Morphees* are capable of providing both tactile and kinesthetic feedback; therefore, they lack comprehensive haptic feedback. This may be attributed to the low force and displacement produced by the piezoelectric actuator (insufficient for kinesthetic feedback) and the slow response of the shape-memory alloy (SMA) actuator (<5 Hz, insufficient for vibrotactile feedback). To produce comprehensive haptic feedback, a device must be capable of providing distinguishable forces and displacements, as well as tactile feedback. Under these constraints, a more suitable actuation basis must be realized; a promising step toward this goal may be through the rapid response and dramatically variable viscosity of smart fluids.

Magnetorheological (MR) fluid–based haptic devices have been developed in recent years (An and Kwon, 2002; Jansen et al., 2010a; Kim et al., 2016). However, reducing the size of MR fluid–based actuators proves to be difficult due to the size requirement of electromagnet coils. To investigate the feasibility of miniaturizing MR fluid–based haptic devices, Yang et al. (2010) proposed a new tunable stiffness display. In subsequent parametric modeling studies, this design was reduced into a miniature button capable of producing a wide range of kinesthetic and vibrotactile feedback (Ryu et al., 2015; Yang et al., 2017). Still, basing an actuator around MR fluid requires precise manufacturing to miniaturize the complex circuitry associated with the solenoid coil.

Electrorheological (ER) fluid, MR fluid's counterpart with a viscosity dependent upon electric field, presents opportunity to address the difficulties of implementing MR fluid in miniature applications. Similar to MR fluid, ER fluid features response times in the order of milliseconds, low power consumption, and few issues with control stability (Bullough et al., 1993; Choi et al., 1997; Han et al., 2000; Stangroom, 1983; Whittle et al., 1996). In addition, with Wen et al.'s (2003) fabrication and modeling of giant electrorheological (GER) fluid, GER fluid–based devices are capable of producing high yield stresses, similar to those of MR fluid–based designs. However, compared to MR fluid, the electrical design for controlling ER fluid is simpler; only two electrodes spaced approximately 1 mm apart are needed, thinner than the equivalent solenoid coil for MR devices. With a goal of actuator mobility, a basis of ER fluid allows for smaller and more portable designs.

While ER fluid has often been applied to exclusively tactile or force feedback devices, research toward comprehensive haptic devices is limited (Fricke, 1993; Goto and Takemura, 2013; Monkman, 1992; Pfeiffer et al., 1999; Taylor et al., 1996; Tsujita et al., 2010). Among these, no designs focus specifically on ER fluid's potential for device minimization. Mazursky et al. (2018) validated this idea experimentally with a small haptic button (14.5 mm thickness) based on ER fluid in flow mode driven by an elastic contact surface. However, this study left room to further reduce the actuator's size and verify its performance mathematically. In the past half-century, several mathematical models have been proposed to approximate the ER fluid's output force based on operating mode, such as flow, shear, and squeeze modes (Burton et al., 1996; Choi and Choi, 1999; Phillips, 1969; Wereley and Pang, 1998). These models are based upon the Bingham plastic behavior of ER fluid. In this study, a pressure-driven flow mode model is presented to characterize the behavior of the proposed haptic actuator.

This study presents a new design for a miniature haptic actuator to overcome the challenges of decreasing the size of kinesthetic devices for mobile integration. The goals of this study are to design an ER fluid–based haptic actuator, to investigate its performance with mathematical modeling, and to experimentally evaluate its ability to produce both kinesthetic and tactile feedback. The actuator is manufactured using printed circuit boards (PCBs) to integrate its electrical and structural components. Within the actuator, ER fluid provides the variable resistive force to the button's kinesthetic interface. By supplying high voltage signals to the electrodes on the PCB, the device's force feedback is controlled. Introducing a frequency into the applied voltage results in oscillations in the kinesthetic response to produce a vibrotactile response. Therefore, the proposed ER fluid–based device is capable of producing haptic feedback.

The next section explains the design methodology and working principles, followed by the fabrication of the prototype. Following the design section, the process of analyzing the device's behavior through math modeling is described. The experiments to measure the force

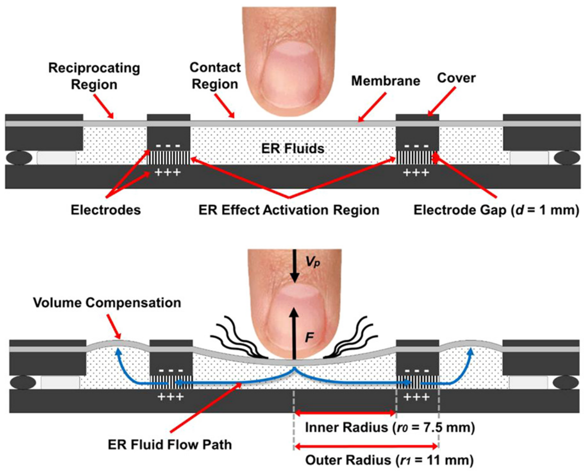

Figure 1. Working principle of the proposed haptic actuator (a) before contact and (b) mid-contact.

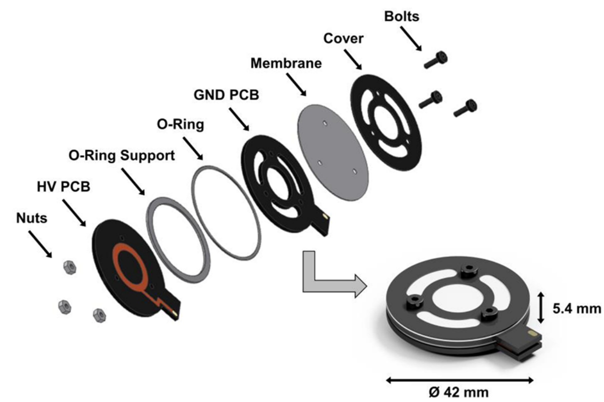

Figure 2. Exploded view drawing of the proposed haptic actuator.

profile over the actuator's stroke are then described in the experimental setup, followed by the experimental results and discussion.

2. Proposed design for a haptic actuator

To design the proposed haptic actuator, the working principles of using ER fluid to produce haptic feedback were established and are first detailed in this section. The structural design of the actuator is then proposed. Finally, the fabricated prototype actuator is presented.

2.1. Working principles

Figure 1 illustrates the cross section and the working principle of the proposed haptic actuator. When pressing the actuator's compliant contact surface, ER fluid flows radially outward through the gap between stationary electrodes, or the activation region. Therefore, it can be said that the actuator operates in pressure-driven flow mode, similar to that of a valve. To compensate for the change in volume due to indentation, radial slots have been included in the GND PCB and cover, allowing the membrane in the slots to expand elastically, creating a reciprocating reservoir (see Figure 1(b)). When pressure on the contact surface is released, the fluid is pushed by the contracting membrane from the reservoir and the device returns to its pre-contact state. When a voltage is applied to the electrodes, the ER fluid in the resultant electric field forms a fibrous network parallel to the field lines. This liquid–solid transition generates a yield stress with magnitude corresponding to the supplied voltage. Therefore, the force felt by the user's finger when pressing directly corresponds to the yield stress produced by the fluid. For a range of supplied voltage magnitudes and frequencies, a range of feedbacks may be felt by the user.

2.2. Structural design

An exploded view of the proposed haptic actuator is presented in Figure 2. The structure is composed of two PCB electrodes and an elastic membrane contact surface. The internal volume of the device contains ER fluid. The bottom PCB has an annulus-type electrode and is rated for high voltages (HV PCB). A plastic ring is fitted between the two PCBs, providing rigidity to the O-ring seal and sets the gap distance between the electrodes to 1 mm. The top PCB has identical electrode geometry to the HV PCB and functions as grounding (GND PCB) for the applied electric field. A compliant silicone membrane (PDMS) is sealed to the top of the GND PCB by a thin layer of acrylic tape (VHB 4910; 3M™) and functions as the device's contact surface. Nylon nuts and bolts fasten the device and compress the O-ring and membrane seals to secure the ER fluid inside. Two tabs allow for HV and GND leads to be secured to the electrode PCBs for electrical inputs. The assembled device has a diameter of 42 mm and a thickness of 5.4 mm.

2.3. Fabrication of a prototype actuator

Figure 3 shows the constructed components and assembly of the prototype actuator. The button-type actuator comprises two electrode PCBs, a plastic spacer and O-ring, a thin film silicone membrane, and a plastic cover. The HV PCB was treated with a thin polyimide film to prevent arcing at high voltages. The electrode's inner and outer radii measure 7.5 and 11 mm, respectively. The internal volume of the actuator is filled with 1.8 mL of giant ER fluid, thus providing potential for greater yield stresses than conventional ER fluid. The maximum indentation depth or stroke of the actuator is 1 mm. The device was designed and manufactured with a goal of minimizing thickness to convey kinesthetic and tactile feedback in miniature applications. The size of the proposed actuator is significantly thinner than

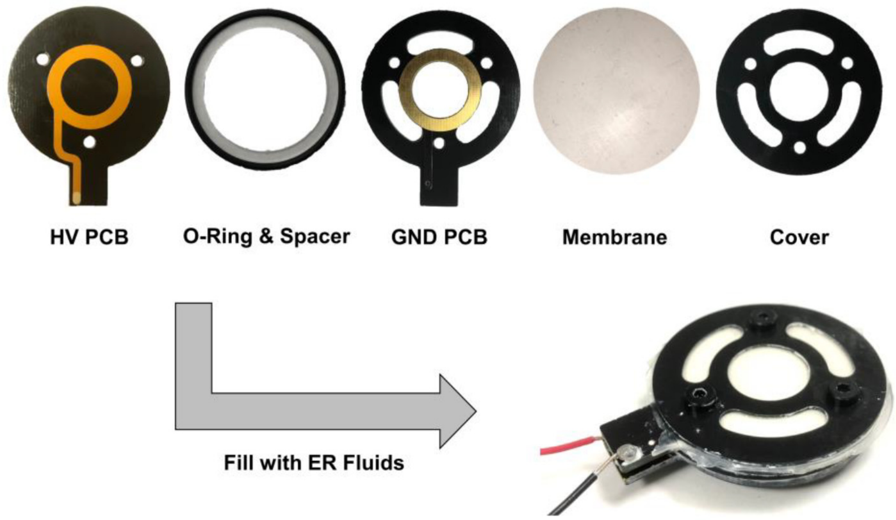

Figure 3. Construction and assembly of the prototype actuator.

previous designs utilizing smart materials (Jansen et al., 2010b; Mazursky et al., 2018; Ryu et al., 2012; Xu et al., 2018). In addition, the design is mechanically simple and easily controlled.

3. Mathematical modeling

To understand the actuator's performance from a mathematical perspective, a model was developed based on the actuator's fundamental behavior. First, an analytical solution to the resistive force produced by the actuator over its stroke as a function of applied electric field was derived. In addition, an analytical representation of the membrane's load–deflection behavior was produced. A numerical approach was taken to simulate the actuator's resistive force output and is presented as well.

3.1. Analytical modeling of ER fluid

To characterize the behavior of the proposed haptic actuator, an analytical model was developed to determine the resistive force produced by the actuator. First, boundary conditions are applied to the Navier–Stokes equation, resulting in the velocity profile of the fluid flow between the plates. Integrating about the electrode area returns the total flow rate. From the volume continuity condition, the flow rate between the plates must be equal to the flow rate due to the indenter; therefore, the pressure gradient may be realized. The pressure gradient is then used to attain the pressure drop across the plates and the contribution of the ER fluid to the resistive force produced by the actuator. Further details to each of these steps are provided with mathematical representations in the following sections.

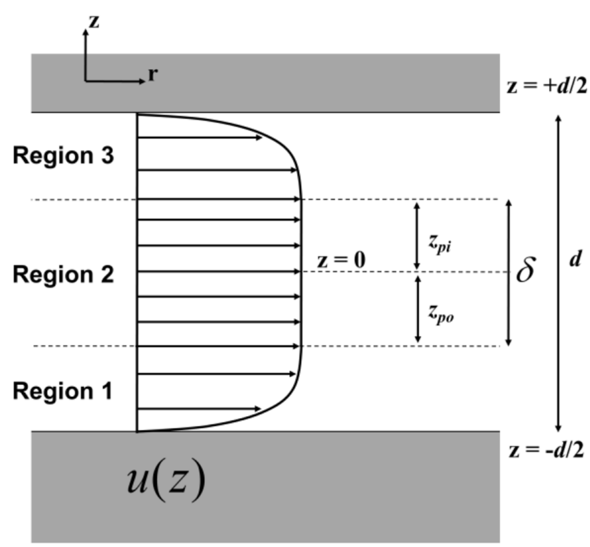

Figure 4. Velocity profile of ER fluid in the activation region associated with a fixed electrode configuration.

3.1.1. Navier–Stokes equation and assumptions. Upon indenting the contact membrane at a rate of V_p, ER fluid flow develops between the parallel electrodes. As shown in Figure 4, the velocity profile in the activation region is composed of three regions due to the Bingham plastic behavior of ER fluid. Flow near the electrode walls (regions 1 and 3) is where the shear stress is greatest and where yield occurs ($|\tau|>\tau_y$). Near the center of the gap (region 2, also known as the plug or core), unyielded fluid flows with a uniform velocity. A parallel plate approximation is made to estimate the annular electrodes as a rectangular duct (Wereley and Pang, 1998).

To find the velocity profile $u(z)$ in flow mode, the Navier–Stokes equation of motion in rectangular coordinates along the x-direction is given

$$\rho\left(\frac{\partial u}{\partial t}+u\frac{\partial u}{\partial x}+v\frac{\partial u}{\partial y}+w\frac{\partial u}{\partial z}\right)=-\frac{dP}{dx}+\rho g_x+\mu\left(\frac{\partial^2 u}{\partial x^2}+\frac{\partial^2 u}{\partial y^2}+\frac{\partial^2 u}{\partial z^2}\right) \tag{1}$$

Applying assumptions of steady flow, unidirectional flow, mass conservation, and omitting gravity leads to the simplified relation between pressure gradient and flow profile

$$\frac{dP}{dx}=\mu\frac{d^2 u}{dz^2} \tag{2}$$

To better illustrate the physical relation to the actuator design, the variable x is renamed to r.

3.1.2. Boundary conditions and flow velocity u in each region. To find the flow velocity in each region, integration is performed and constants are determined by applying boundary conditions (no-slip, uniform flow in region 2)

$$\begin{aligned} u_1 &= \frac{1}{2\mu}\frac{dP}{dr}\left[\left(z+z_{po}\right)^2-\left(\frac{d}{2}-z_{po}\right)^2\right] \\ u_2 &= -\frac{1}{2\mu}\frac{dP}{dr}\left(\frac{d}{2}-z_{pi}\right)^2 \\ u_3 &= \frac{1}{2\mu}\frac{dP}{dr}\left[\left(z-z_{pi}\right)^2-\left(\frac{d}{2}-z_{pi}\right)^2\right] \end{aligned} \tag{3}$$

3.1.3. Total flow rate Q. Knowing $u(z)$, volumetric flow rate Q across the electrode area A may be found using

$$Q=\int_{2\pi r_0}^{2\pi r_1}\int_{-\frac{d}{2}}^{\frac{d}{2}}(u)dzdr \tag{4}$$

where r_1 and r_0 are the outer and inner electrode radii, respectively. This integration is performed separately for each region

$$\begin{aligned} Q_1 &= \frac{\pi}{12\mu}\frac{dP}{dr}(d-\delta)^3(r_0-r_1) \\ Q_2 &= \frac{\pi\delta}{4\mu}\frac{dP}{dr}(d-\delta)^2(r_0-r_1) \\ Q_3 &= \frac{\pi}{12\mu}\frac{dP}{dr}(d-\delta)^3(r_0-r_1) \end{aligned} \tag{5}$$

Knowing that Q_{total} is the sum of the regional flow rates and simplifying yields

$$Q_{\text{total}}=Q_1+Q_2+Q_3=\frac{\pi}{12\mu}\frac{dP}{dr}(d-\delta)^2(2d+\delta)(r_0-r_1) \tag{6}$$

3.1.4. Pressure gradient dP/dr. To solve for the pressure gradient, the conservation of incompressible mass flow rate condition is utilized

$$Q_{\text{total}}=Q_p \tag{7}$$

where $Q_p=V_pA_p(d_i)$ is the flow rate due to the membrane's displacement. Substituting equation (7) into equation (6)

$$V_pA_p=\frac{\pi}{12\mu}\frac{dP}{dr}(d-\delta)^2(2d+\delta)(r_0-r_1) \tag{8}$$

To reduce the unknown quantities, the plug thickness δ must be derived. Examining the hydrostatic force balance on a volume element and simplifying yields

$$\delta=-\frac{2\tau_y}{dP/dr} \tag{9}$$

In addition, for the given geometry, the pressure differential may be written as

$$\frac{dP}{dr}=-\frac{\Delta P}{r_1-r_0} \tag{10}$$

Substituting equations (9) and (10) into equation (8) results in the equation of pressure gradient

$$V_pA_p=\frac{\Delta P}{12\mu}\left(2d-\frac{2\tau_y(r_0-r_1)}{\Delta P}\right)\left(d+\frac{2\tau_y(r_0-r_1)}{\Delta P}\right)^2 \tag{11}$$

Upon simplification, a modification to the classical result produced by Phillips (1969) is found specific to the actuator's geometry

$$\Delta P=\frac{8\mu V_pA_p}{2\pi r d^3}+2\frac{r_1-r_0}{d}\tau_y \tag{12}$$

3.1.5. Resistive force F_{ER}. Finally, to determine the resistive force felt by the user due to the flow mode of the ER fluid, the pressure drop across the electrodes is multiplied by the area of the indenter

$$F=\Delta PA_p \tag{13}$$

For a membrane-based contact surface, the indenter or finger area varies with depth, resulting in a nonlinear volumetric flow rate. Therefore, the volumetric flow may be approximated

$$A_p=\pi r_{pf}^2\frac{\delta_i}{\delta_f} \tag{14}$$

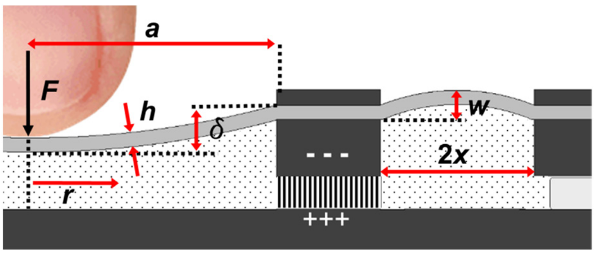

Figure 5. Schematic diagram of the dimensions used in the membrane load–deflection analysis.

where r_{pf} is the final radius of the indenter. The dimensionless δ_i/δ_f term compares the current indentation depth to the final depth.

3.2. Analytical modeling of membrane mechanics

The resistive force represented by equation (13) only accounts for the force due to the ER fluid's performance. When a user interacts with the proposed button-type actuator, additional resistive forces are present due to the elastic force of the membrane. This force is produced through both contact and the resulting reciprocation, as shown in Figure 5. An analytical model for the force generated through the membrane's elastic deformation is produced based on derivations by Komaragiri and Vlassak (Komaragiri et al., 2005; Vlassak and Nix, 1992). As described in section 2.2, the membrane consists of two layers: contact and adhesive. The contact layer of the membrane, made of PDMS, is taken to behave as a nonlinear membrane without pre-strain, while the adhesive layer of the membrane, made of acrylic tape (VHB 4910; 3M), is taken to behave as a linear, pre-stretched membrane. By superposing the force–displacement curves produced by each layer, the analytical result may accurately capture the experimental behavior and provide a complete theoretical model of the actuator's performance.

3.2.1. Nonlinear PDMS layer (without pre-strain). First, the circular contact membrane is examined. An approximate solution to the midpoint deflection of a thin, circular membrane without pre-strain is given (Komaragiri et al., 2005)

$$\frac{\delta}{a} = g(\nu)\left(\frac{pa}{Eh}\right)^{1/3} \tag{15}$$

where δ is the midpoint deflection, p is the applied pressure, a is the radial span, E is the elastic modulus, h is the thickness of the membrane, and $g(\nu) \approx 0.7179 - 0.1706\nu - 0.1495\nu^2$. Since the proposed study describes a strain-controlled model and experiment, the pressure as a result of strain is of interest. Rearranging yields

$$p = \frac{E\delta^3 h}{a^4 g(\nu)^3} \tag{16}$$

The reciprocating membrane is approximated as three rectangular films. The load–deflection relation for high aspect ratio films may be represented as (Vlassak and Nix, 1992)

$$q = \frac{4Eh}{3x^4(1-\nu^2)}w^3 \tag{17}$$

where x is the membrane width, w is the deflection at the midpoint of the reciprocating membrane, and q is the pressure on the reciprocating membrane. Deflection at the midpoint of the reciprocating membrane is related to the contact membrane deflection by conservation of volume.

3.2.2. Linear VHB layer (pre-strained). An approximate solution to the midpoint deflection of a thin, circular membrane with pre-strain is given (Komaragiri et al., 2005)

$$\delta = a\int_1^0 \beta(\bar{r})d\bar{r} \tag{18}$$

where angle of rotation β is defined

$$\beta(\bar{r}) = -\frac{6(1-\upsilon^2)}{\kappa^2}\left(\frac{pa^3}{Eh^3}\right)\left[\bar{r} - \frac{I_1(k\bar{r})}{I_1(k)}\right] \tag{19}$$

where I_1 denotes Bessel's function of the first kind. The terms κ, k, and $\bar{r}$ are defined as

$$\begin{aligned} \kappa^2 &= 12\varepsilon_0(1+\nu)\left(\frac{a}{h}\right)^2 \\ k &= (1-\nu)^{-1} \\ \bar{r} &= \frac{a}{r} \end{aligned} \tag{20}$$

where ε_0 is the pre-strain and r is radial position. This system of equations is evaluated to find pressure as a result of applied strain.

Similarly, the load–deflection relation for a pre-stretched rectangular membrane with high aspect ratio is shown to be (Vlassak and Nix, 1992)

$$q = 2\frac{\sigma_0 h}{x^2}w + \frac{4Eh}{3x^4(1-\nu^2)}w^3 \tag{21}$$

where σ_0 is the pre-stress.

By relating pressure to force through the corresponding membrane areas, the total force due to the elastic membrane is realized. Therefore, the complete kinesthetic force felt by the user may be represented by

$$F_{\text{total}} = F_{\text{Field-dependent ER force}} + F_{\text{membrane}} \tag{22}$$

Table 1. Parameters of the proposed haptic actuator.

Parameter	Symbol	Value
Electrode gap	d	1 mm
Electrode radius (inner)	r_0	7.5 mm
Electrode radius (outer)	r_1	11 mm
Viscosity of GER fluid	μ	0.060 Pa s
Diameter of indenter	D_p	11.8 mm
Velocity of indentation	V_p	1 mm/s

GER: giant electrorheological.

Table 2. Parameters of the membrane model.

Parameter	Symbol	Value (PDMS)	Value (VHB)
Radial span	a	7.5 mm	7.5 mm
Width	x	2.34 mm	2.34 mm
Thickness	h	0.43 mm	0.08 mm
Pre-strain	ε_0	0	0.065
Pre-stress	σ_0	0	50 kPa
Elastic modulus	E	350 kPa	60 kPa
Poisson's ratio	ν	0.50	0.49

where the force due to the elastic membrane F_{membrane} consists of forces at both the contact surface and reciprocating reservoir. By changing the magnitude and frequency of the input voltage, the magnitude of the ER effect, and therefore resistive force, can be controlled in real time resulting in a range of kinesthetic and vibrotactile sensations.

3.3. Numerical evaluation of the proposed actuator

To simulate the actuator's behavior, a MATLAB® script was developed based on the modeling presented in the previous section to calculate the forces produced over the actuator's stroke. The model accounts for both the force produced by the elastic contact surface and the ER fluid effect. A coupling between the applied electric field and the giant ER fluid's yield stress was established using properties provided by the manufacturer (Smart Materials Laboratory Ltd), such as a maximum yield stress of 80 kPa at 5 kV/mm, and was represented with the GER scaling function (Vemuri et al., 2012). The yield stress due to the electric field is used as an input to determine the ER actuator force. Parameters critical to the numerical simulation of the ER effect and membrane kinematics are provided in Tables 1 and 2, respectively. Values used reflect the properties of the fabricated actuator and the experimental test setup.

The membrane's force–displacement behavior was simulated by imposing indentation from 0 to 1 mm at the center of the contact membrane and calculating the resulting force, shown in Figure 6. As shown, the pre-strained acrylic tape layer (VHB) responds linearly while the relaxed contact layer (PDMS) exhibits nonlinear behavior. Together, the two layers contribute to the total combined membrane response. At the bottom of the stroke, the contact and reciprocating membranes contribute about 0.5 and 2.1 N, respectively. The combined membrane performance is utilized in the complete numerical simulation of the actuator performance.

The simulation takes applied voltage and frequency as inputs and produces plots of the force generated by the actuator along its indentation stroke. Figure 7(a) shows the force profiles predicted by the simulation when subjected to DC voltage inputs of 0, 1, 2, 3, and 4 kV. As shown, when no power is supplied to the actuator (0 kV, or off-state), the maximum force produced is about 2.5 N at the bottom of the stroke. When the maximum voltage is supplied (4 kV DC), the maximum force increases to nearly 3.6 N. Figure 7(b) shows the force profiles predicted when the model is subjected to

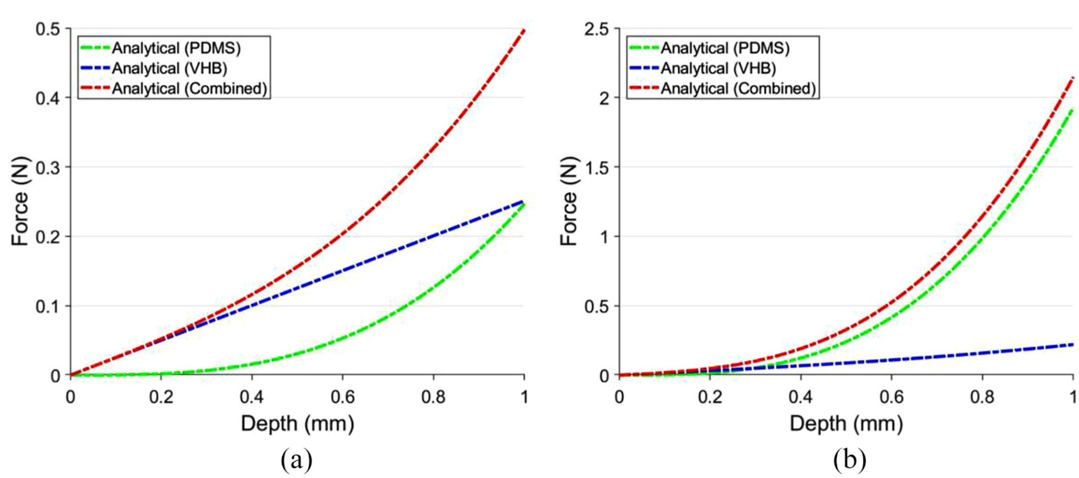

Figure 6. Simulation results for the force produced by indenting the superposed membrane in the (a) contact and (b) reciprocating regions.

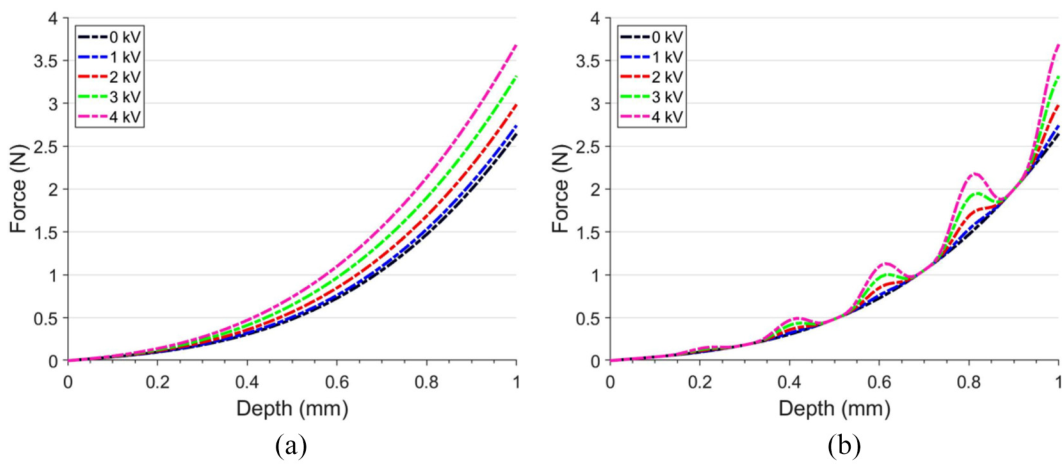

Figure 7. Results of the simulated actuator: force (N) versus depth (mm) along its stroke when subjected to (a) various DC voltages and (b) 5 Hz sine functions.

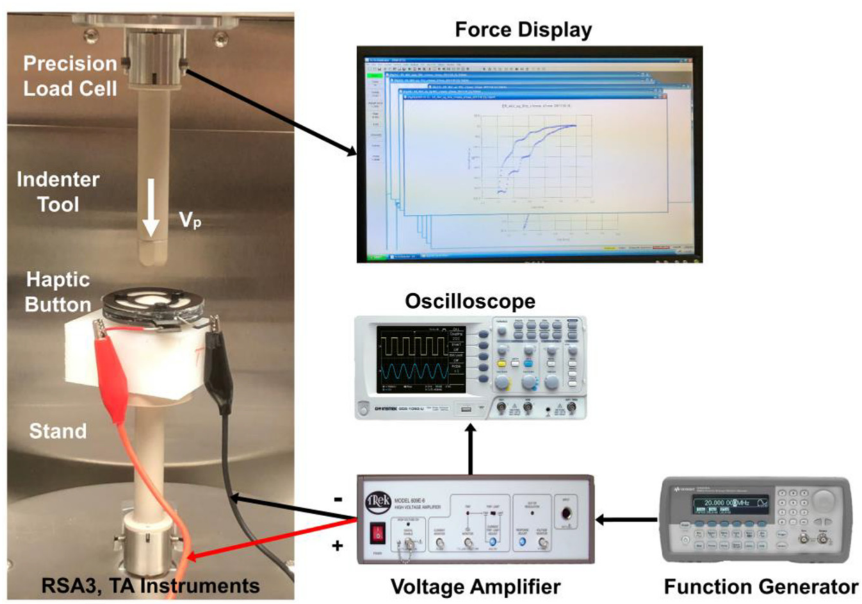

Figure 8. Experimental setup to measure the force generated by the prototype actuator with respect to indentation depth for applied voltage signals.

sinusoidal excitation between 0 V and 1, 2, 3, and 4 kV at a frequency of 5 Hz. It is seen that as the magnitude of the voltage increases, the amplitude of vibration increases. Therefore, the simulation implies that the design is capable of providing both kinesthetic and vibrotactile feedback.

4. Experimental evaluation

This section presents the experimental methods for testing the fabricated haptic device and analysis of the experimental results. The goal of the experimental analysis is to measure the device's ability to produce a significant range of kinesthetic and vibrotactile sensations. An experimental method of measuring the actuator's output with respect to depth for voltage inputs is described.

4.1. Experimental setup

To evaluate the performance of the fabricated haptic actuator, mechanical analysis was conducted using a dynamic mechanical analyzer (RSA3; TA Instruments), function generator, and voltage amplifier, as shown in Figure 8. This experimentation precisely measured the total resistive force with respect to indentation depth

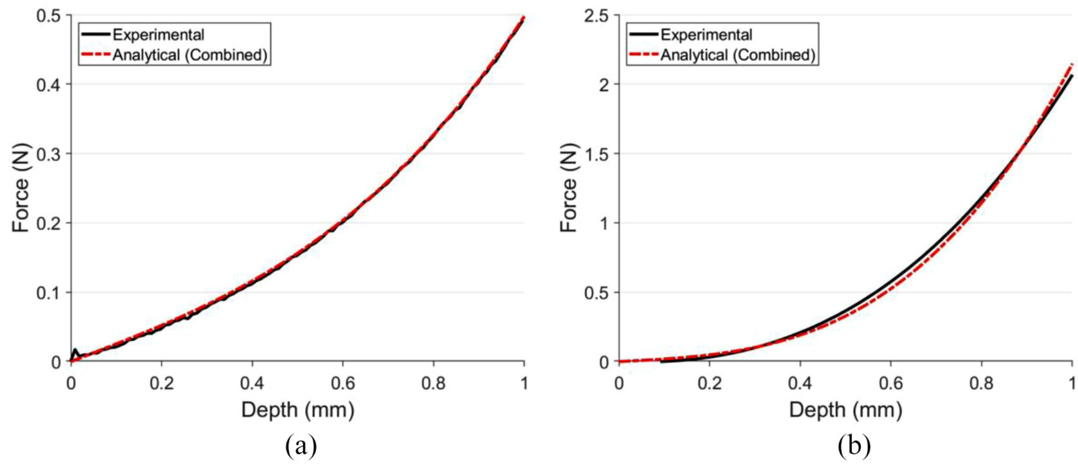

Figure 9. Comparison between the membrane's experimental performance from dry testing and the analytical response for the (a) contact membrane and (b) reciprocating membrane.

over the device's 1 mm stroke. The performance was evaluated under different input voltage and frequency conditions using an indenter similar in size to a human finger. An indentation rate of 1 mm/s was used.

4.2. Membrane response

To first validate the modeled membrane's response, dry testing was performed with an assembled actuator containing no ER fluid. Figure 9 compares the simulated and experimental membrane response. The analytical membrane model is demonstrated to be sufficiently accurate when plotted against the experimental response.

4.3. Kinesthetic response

To test the actuator's ability to produce a range of stiffnesses, the actuator's resistive force was first measured in its off-state. Then, a high-frequency square wave was applied between 0 V and peak amplitudes of 1, 2, 3 and 4 kV to emulate a pulsating DC signal. These results are presented in Figure 10. As evidenced in the figure, as the magnitude of the input voltage and pressed depth increase, the resistive force increases. The off-state resistive force was measured to be about 2.5 N at maximum depth. The maximum force produced was about 3.6 N under 4 kV load. While the force profiles formed by voltages up to 3 kV had similar curvature, the force curve produced under the 4 kV input included a steep increase and decrease in force during the 0.3–0.5 mm range of the stroke. This can be attributed to a build-up of pre-yield ER fluids in the activation region, followed by a rapid yielding event.

In addition, Figure 10 compares the experimental results (opaque, smooth lines) with the results of the kinesthetic numerical simulation (transparent, dashed lines). The simulation and experimental results agree acceptably well. The off-state, 1, 2, and 3 kV results overlay with little variance. The 4 kV responses differ due to the yielding event observed in experiments not being included in the model. However, the maximum force produced by the actuator was accurately determined by the mathematical model.

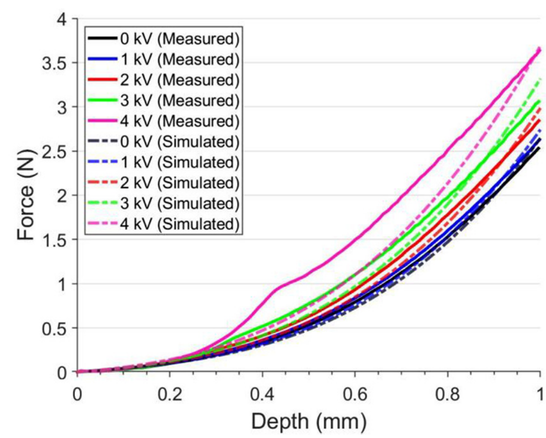

Figure 10. Comparison of kinesthetic feedback between the measured force and simulated force.

To further examine the results from a haptic perspective, the just-noticeable difference (JND) must be calculated. The JND is a measure of the amount that the kinesthetic force must change for a difference to be perceived by a human. For kinesthetic feedback, force rate is the metric for JND. Force rate (Q_v) at a given depth is defined as the ratio of the difference between the maximum and minimum force (P_v) to the maximum force (L_v) at said depth

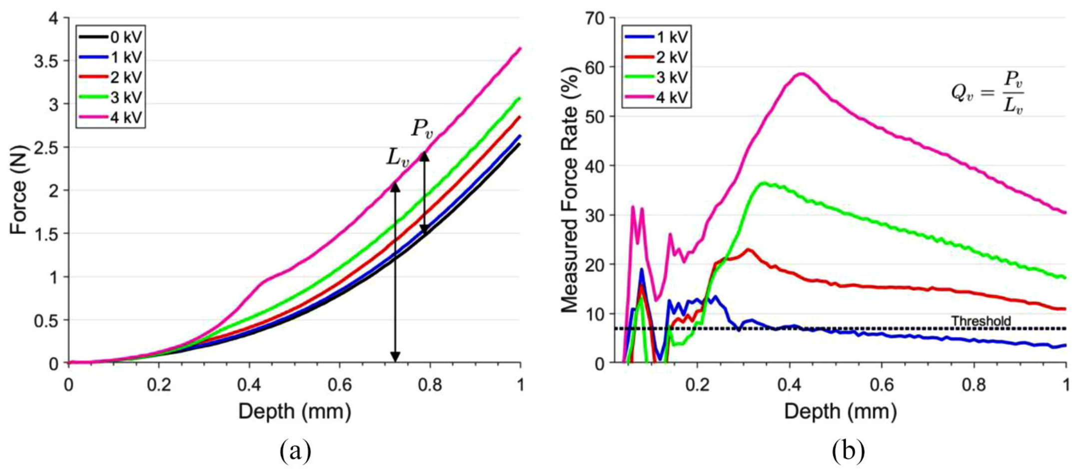

Figure 11. Results of kinesthetic evaluation: (a) force vs. depth and (b) translated to force rate vs. depth.

$$Q_v = \frac{P_v}{L_v} \tag{23}$$

Figure 11(b) is produced by applying equation (23) across all given depths in the actuator's stroke. From an indentation depth of 0–0.2 mm, some volatility occurs due to the relatively low magnitudes of the forces, as evidenced in Figure 10. From 0.2 to 1 mm, the force rates stabilize and follow a similar trend; force rate increases with respect to applied voltage. Beyond 0.2 mm, the lowest force rate is about 3.5% at a depth of 1 mm under 1 kV applied signal. The greatest force rate of 58.5% is produced at maximum voltage and occurs at about 0.4 mm indentation depth, corresponding to the yielding event observed in Figure 10. The threshold for which humans can consistently detect changes in force is about 7%–10% for forces between 0.5 and 200 N (Pang et al., 1991). As indicated by the plot in Figure 11(b), the proposed actuator is capable of conveying distinct haptic feedback above the threshold for supplied voltages greater than 1 kV.

4.5. Tactile response

To demonstrate a vibrotactile response, sinusoidal voltage inputs were applied between 0 V and peak amplitudes of 1, 2, 3, and 4 kV and at frequencies of 1, 3, 5, and 10 Hz. Figure 12 presents the resultant force profiles for each set of frequencies and voltages. As seen in the figure, the force feedback responds harmonically when subjected to sinusoidal voltages. As the magnitude of the applied voltage increases, the amplitude of vibration increases as well. These results show that the actuator can convey controllable resistive forces over a range of frequencies. Therefore, the actuator is capable of communicating vibrotactile feedback.

To further demonstrate the proposed numerical model's accuracy, its response to a sinusoidal excitation is compared to the measured response for 3 Hz, shown in Figure 13. Specifically, emphasis is placed on the force due to the fluid by removing the elastic membrane's response. As shown in the figure, the predicted vibrotactile response is similar to that measured in experiments. It is seen that at indentation depths greater than ˜0.7 mm, the model tends to overestimate the force due to the ER effect.

5. Conclusion

This article has presented the design, modeling, and experimental evaluation of a novel design for a miniature haptic actuator based on the tunable yield stress of ER fluids. The device was designed in flow mode to minimize actuator thickness and mechanical complexity. An analytical model for the actuator's force output was derived and implemented into a numerical simulation. A prototype actuator was fabricated and tested experimentally using a dynamic mechanical analyzer. The resistive force generated by the actuator along its stroke was measured for both kinesthetic and vibrotactile input voltage signals. The experimental results verified those produced by the model. The results indicated that the actuator's resistive force increases with increased indentation depth and applied voltage. Furthermore, the measured results demonstrate distinct force rates that may be perceived by humans as a range of kinesthetic sensations in application. The vibrotactile performance of the actuator showed significant improvement over previous iterations. Thus, the actuator was confirmed capable of conveying a range of haptic feedback sensations. Future work will include embedding a thin pressure sensor and feedback control

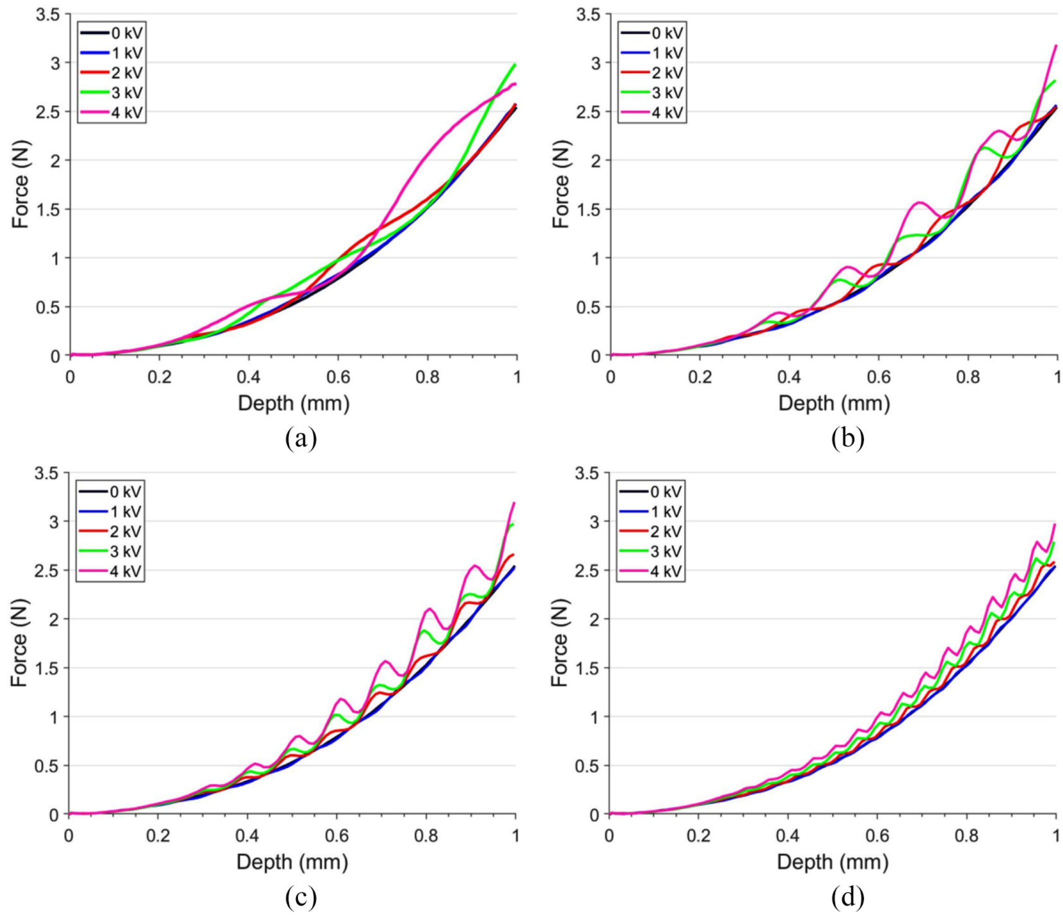

Figure 12. Results of the experimental measurement of the proposed actuator subjected to sinusoidal inputs at (a) 1 Hz, (b) 3 Hz, (c) 5 Hz, and (d) 10 Hz.

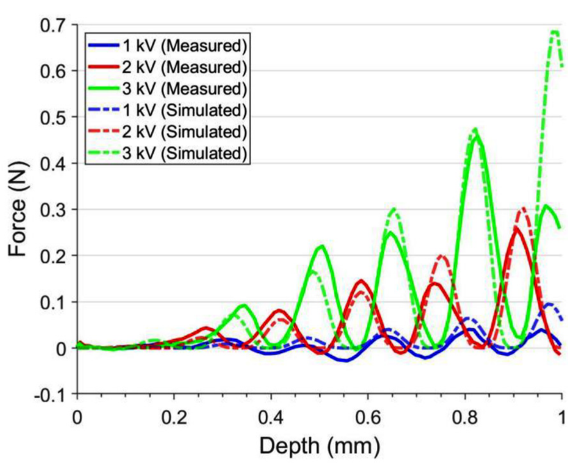

Figure 13. Comparison of vibrotactile feedback strictly due to the ER effect at 3 Hz excitation between the measured force and simulated force.

to act as a haptic interface by rendering realistic sensations between a user and virtual environment.

Declaration of conflicting interests

The author(s) declared no potential conflicts of interest with respect to the research, authorship, and/or publication of this article.

Funding

The author(s) disclosed receipt of the following financial support for the research, authorship, and/or publication of this article: This work was supported by the National Research Foundation of Korea (NRF) grant funded by the Korea Government (MSIT) (No. 2018R1C1B5043837). The financial support is greatly appreciated.

ORCID iD

Jeong-Hoi Koo https://orcid.org/0000-0001-7740-8678

References

Adams RJ, Moreyra MR and Hannaford B (1998) Stability and performance of haptic displays: theory and experiments. In: *Proceedings ASME international mechanical engineering congress and exhibition*, Anaheim, CA, pp. 227–234. Available at: https://pdfs.semanticscholar.org/3fe5/ba2caf483c66f3a463eb9b32238580ae66ee.pdf

An J and Kwon D-S (2002) Haptic experimentation on a hybrid active/passive force feedback device. In: *Proceedings 2002 IEEE international conference on robotics and automation*, pp. 4217–4222. Available at: https://ieeexplore.ieee.org/document/1014416

An J and Kwon D-S (2006) Stability and performance of haptic interfaces with active/passive actuators—theory and experiments. *The International Journal of Robotics Research* 25(11): 1121–1136.

Bianchi M, Scilingo EP, Serio A, et al. (2009) A new softness display based on bi-elastic fabric. In: *Proceedings of third joint eurohaptics conference and symposium on haptic interfaces for virtual environment and teleoperator systems*, pp. 382–383. Available at: https://ieeexplore.ieee.org/document/4810905

Bullough WA, Johnson AR, Hosseini-Sianaki A, et al. (1993) The electro-rheological clutch: design, performance characteristics and operation. *Proceedings of the Institution of Mechanical Engineers, Part I: Journal of Systems and Control Engineering* 207(2): 87–95.

Burton SA, Makris N, Konstantopoulos I, et al. (1996) Modeling the response of ER damper: phenomenology and emulation. *Journal of Engineering Mechanics* 122: 897–906.

Choi S-B and Choi Y-T (1999) Sliding mode control of a shear-mode type ER engine mount. *KSME International Journal* 13(1): 26–33.

Choi SB, Cheong CC, Jung JM, et al. (1997) Position control of an ER valve-cylinder system via neural network controller. *Mechatronics* 7(1): 37–52.

Coles TR, Meglan D and John NW (2011) The role of haptics in medical training simulators: a survey of the state of the art. *IEEE Transactions on Haptics* 4(1): 51–66.

Fricke J (1993) *Tactile graphic computer screen and input tablet for blind persons using an electrorheological fluid.* Patent 5222895, USA.

Fujita K and Ohmori H (2001) A new softness display interface by dynamic fingertip contact area control. In: *Proceedings of the 5th world multiconference on systemics, cybernetics and informatics*, Orlando, FL, 22–25 October 2001, pp. 78–82. IIIS.

Goto M and Takemura K (2013) Tactile bump display using electro-rheological fluid. In: *IEEE international conference on intelligent robots and systems*, pp. 4478–4483. Available at: https://ieeexplore.ieee.org/document/6697000

Han S-S, Choi S-B and Cheong C-C (2000) Position control of X-Y table mechanism using electro-rheological clutches. *Mechanism and Machine Theory* 35(11): 1563–1577.

Jansen Y, Karrer T and Borchers J (2010a) MudPad: localized tactile feedback on touch surfaces. In: *Proceedings of the 23rd annual ACM symposium on user interface software and technology*, pp. 385–386. Available at: https://dl.acm.org/citation.cfm?id = 1866232

Jansen Y, Karrer T and Borchers J (2010b) MudPad: tactile feedback and haptic texture overlay for touch surfaces. *Proceedings of ACM international conference on ITS*, pp. 11–14. Available at: https://dl.acm.org/citation.cfm? id = 1936655

Kim S, Kim P, Park C-Y, et al. (2016) A new tactile device using magneto-rheological sponge cells for medical applications: experimental investigation. *Sensors and Actuators A: Physical* 239: 61–69.

Komaragiri U, Begley MR and Simmonds JG (2005) The mechanical response of freestanding circular elastic films under point and pressure loads. *Journal of Applied Mechanics* 72(2): 203–212.

Laycock S and Day A (2003) Recent developments and applications of haptic devices. *Computer Graphics Forum* 22(2): 117–132.

Mazursky AJ, Koo J-H and Yang T-H (2018) Experimental evaluation of a miniature haptic actuator based on electrorheological fluids. In: *SPIE smart structures and nondestructive evaluation*, Denver, CO, 15 March.

Monkman GJ (1992) An electrorheological tactile display. *Presence: Teleoperators and Virtual Environments* 1(2): 219–228.

Nakagawa Y, Kamimura A and Kawaguchi Y (2012) MimicTile: a variable stiffness deformable user interface for mobile devices. In: *Proceedings of the 2012 ACM annual conference on human factors in computing systems*, pp. 745–748. Available at: https://dl.acm.org/citation.cfm?id = 2207782

Pang XD, Tan HZ and Durlach NI (1991) Manual discrimination of force using active finger motion. *Perception & Psychophysics* 49(6): 531–540.

Park J and Khatib O (2006) A haptic teleoperation approach based on contact force control. *The International Journal of Robotics Research* 25(5–6): 575–591.

Pfeiffer C, Mavroidis C, Bar-Cohen Y, et al. (1999) Electrorheological fluid based force feedback device. In: *Proceedings of the 1999 SPIE telemanipulator and telepresence technologies VI*, pp. 88–99. Available at: https://www.spiedigitallibrary.org/conference-proceedings-of-spie/3840/0000/Electrorheological-fluid-based-force-feedback-device/10.1117/12.369269.short

Phillips RW (1969) *Engineering Applications of Fluids with a Variable Yield Stress*. Berkeley, CA: University of California, Berkeley.

Poupyrev I and Maruyama S (2003) Tactile interfaces for small touch screens. In: *Proceedings of the 16th annual ACM symposium on user interface software and technology*, pp. 217–220. Available at: https://dl.acm.org/citation.cfm?id = 964721

Poupyrev I, Maruyama S and Rekimoto J (2002) Ambient touch: designing tactile interfaces for handheld devices. In: *Proceedings of the 15th annual ACM symposium on user interface software and technology*, pp. 51–60. Available at: https://dl.acm.org/citation.cfm?id = 571993

Rekimoto J and Schwesig C (2006) PreSenseII: bi-directional touch and pressure sensing interactions with tactile feedback. In: *CHI '06 extended abstracts on human factors in computing systems—CHI EA '06*, pp. 1253–1258. Available at: https://www2.sonycsl.co.jp/person/rekimoto/papers/chi06-presense.pdf

Roudaut A, Karnik A, Löchtefeld M, et al. (2013) Morphees: toward high "shape resolution" in self-actuated flexible mobile devices. In: *Proceedings of the SIGCHI conference on human factors in computing systems—CHI '13*, pp. 593–602. Available at: https://dl.acm.org/citation.cfm?id = 2470738&dl = ACM&coll = DL

Ryu S, Koo J-H, Yang T-H, et al. (2015) Mechanical and psychophysical performance evaluation of a haptic actuator based on magnetorheological fluids. *Journal of Intelligent Material Systems and Structures* 27(14): 1967–1975.

Ryu S, Yang TH, Kim SY, et al. (2012) Design of a new miniature haptic button based on magneto-rheological fluids. In: *IEEE international conference on automation science and engineering*, pp. 121–124. Available at: https://www.computer.org/csdl/proceedings/case/2012/0430/00/06386463-abs.html

Song A, Morris D and Colgate JE (2005) Haptic telemanipulation of soft environment without direct force feedback. In: *Proceedings of the 2005 IEEE international conference on information acquisition*, pp. 21–25. Available at: https://ieeexplore.ieee.org/document/1635047

Srinivasan MA and Basdogan C (1997) Haptics in virtual environments: taxonomy, research status, and challenges. *Computers & Graphics* 21(4): 393–404.

Stangroom J (1983) Electrorheological fluids. *Physics in Technology* 14: 290–296.

Taylor PM, Hosseini-Sianaki A and Varley CJ (1996) An electrorheological fluid-based tactile array for virtual environments. In: *Proceedings of 1996 IEEE international conference on robotics and automation*, pp. 18–23. Available at: https://ieeexplore.ieee.org/document/503567

Tsujita T, Kobayashi M and Nakano M (2010) Design and development of a Braille display using micro actuators driven by ER suspension. *International Journal of Applied Electromagnetics and Mechanics* 33(3–4): 1661–1669.

Vemuri SH, Jhon MS, Zhang K, et al. (2012) New analysis of yield stress on giant electrorheological fluids. *Colloid and Polymer Science* 290(2): 189–192.

Vlassak JJ and Nix WD (1992) A new bulge test technique for the determination of Young's modulus and Poisson's ratio of thin films. *Journal of Materials Research* 7(12): 3249–3342.

Wen W, Huang X, Yang S, et al. (2003) The giant electrorheological effect in suspensions of nanoparticles. *Nature Materials* 2: 727–730.

Wereley NM and Pang L (1998) Nondimensional analysis of semi-active electrorheological and magnetorheological dampers using approximate parallel plate models. *Smart Materials and Structures* 7: 732–743.

Whittle M, Atkin RJ and Bullough WA (1996) Dynamics of an electrorheological valve. *International Journal of Modern Physics B* 10(23–24): 2933–2950.

Xu L, Li Y, Han L, et al. (2018) A test of giant electrorheological valve in DC and square wave AC fields with different frequencies. *Journal of Intelligent Material Systems and Structures* 29(2): 250–254.

Yang TH, Koo JH, Kim SY, et al. (2017) Modeling and test of a kinaesthetic actuator based on MR fluid for haptic applications. *The Review of Scientific Instruments* 88(3): 035004.

Yang TH, Kwon H-J, Lee SS, et al. (2010) Development of a miniature tunable stiffness display using MR fluids for haptic application. *Sensors and Actuators A: Physical* 163(1): 180–190.